Franz-Keldysh effect and dynamical Franz-Keldysh effect of cylindrical quantum wires

T. Y. Zhang and W. Zhao

*State Key Laboratory of Transient Optics and Photonics, Xi'an Institute of Optics and Precision Mechanics, Chinese Academy
of Sciences, 322 West Youyi Road, Xi'an 710068, People's Republic of China*
(Received 18 November 2005; revised manuscript received 24 March 2006; published 29 June 2006)

We investigate the interband optical absorption spectra near the band edge of a cylindrical semiconductor quantum wire in the presence of a static electric field and a terahertz electric field polarized along the axis. Optical absorption spectra are nonperturbatively calculated by solving the low-density semiconductor Bloch equations in real space and real time. The influence of the Franz-Keldysh (FK) effect and dynamical FK effect on the absorption spectrum is investigated. To highlight the physics behind the FK effect and dynamical FK effect, the spatiotemporal dynamics of the polarization wave packet are also presented. Under a reasonable static electric field, substantial and tunable absorption oscillations appear above the band gap. A terahertz field, however, will cause the Autler-Townes splitting of the main exciton peak and the emergence of multiphoton replicas. The presented results suggest that semiconductor quantum wires have potential applications in electro-optical devices.

I. INTRODUCTION

Excitons, which are bound states of electrons and holes due to the attractive Coulomb interaction between them, play a much more important role in low-dimensional semiconductor nanostructures than they do in three-dimensional bulk semiconductors. The quantum confinement of the excitons on length scales smaller than the bulk Bohr radius leads to enhanced exciton peaks in optical absorption spectra of low-dimensional nanostructures.[1–4] Extensive work has been done to investigate the specifics of the excitonic optical properties of quantum wells,[1,2] quantum wires,[3–6] quantum dots,[7–10] and superlattices. [11–16] The optical spectra of semiconductor structures can be modified dramatically by the application of external static electric and/or magnetic fields. For semiconductor quantum wells, the Franz-Keldysh (FK) effect occurs when an electric field polarized in the plane of the quantum wells is applied, while the quantum-confined Stark effect prevails for a field polarized in the growth direction.[2] The FK effect describes the nonvanishing optical absorption below the band gap as well as characteristic oscillations above the gap.[17,18] And the quantum-confined Stark effect describes the strong spectral shifts of the optical absorption edge with the applied electric field. In recent years, excitonic absorption in low-dimensional semiconductor nanostructures driven by terahertz ac electric fields has attracted a great deal of attention[19–29] due to the availability of strong coherent terahertz sources, such as free-electron lasers. Many interesting optical phenomena have been predicted theoretically and partly verified experimentally, such as the ac Stark effect, the dynamical FK effect,[19,20] dynamical localization, and terahertz sideband generation.[30]

Semiconductor quantum wires have attracted considerable attention due to their distinct optical and electronic properties, which have potential applications in novel optoelectronic devices. Quantum wires also offer a unique opportunity for investigating the kinetics of electrons and holes in one-dimensional structures.[3] A unique feature of the one-dimensional system is the inverse-square-root divergence of the joint density of states at the band edge. However, the Coulomb interactions between electrons and holes remove this divergence and reduce the Sommerfield factor, which is the intensity ratio of the optical density associated with excitonic scattering states to the free-electron–hole pairs above the band gap.[4] Consequently, the singular one-dimensional joint density of states does not show up at all in the linear absorption spectrum. Moreover, in contrast to the two-dimensional and three-dimensional cases, the Sommerfield factor is less than unity for all frequencies above the band gap. With rapid advance in material growth technology, both experimental[31–35] and theoretical[36–41] studies on semiconductor quantum wires are receiving renewed interest. These studies are important not only for elucidating the fundamental physics of one-dimensional semiconductors, but also for device applications of quantum wires.

In this paper, we investigate the FK effect and dynamical FK effect in a cylindrical semiconductor quantum wire. We explore the optical polarization and its dephasing dynamics by solving the semiconductors Bloch equations (SBEs) in the low-density limit in real space. In general, the SBEs are solved in k space.[5,26] However, solving the SBE in k space is much more formidable in numerical implementation, especially when external fields are applied. The advantages of the real-space approach are as follows: (i) it can be used as a probe into the wave-packet motion of the polarization, (ii) the Coulomb singularity can be resolved analytically by a polynomial finite element, (iii) bound, quasibound, and free states are included in the calculation, (iv) external fields can be added conveniently, and (v) it can be incorporated to implement a very efficient fast Fourier transform algorithm. Hence, solving the SBEs in real space began to attract great interest recently.[16,27–29,42–44] Hughes and Citrin have used this approach to investigate the FK effect, the terahertz dynamical FK effect, and ionization of excitons in semiconductor quantum-well wires where the lateral confinement potential is assumed to be a harmonic-oscillator potential.[42,43] Since we concern the spatiotemporal evolution of the polarization wave packets, the real-space approach is adopted in this paper. The paper is organized as follows. In Sec. II, we

outline our model of the cylindrical quantum wire and theoretical approach used to obtain the optical absorption spectrum. In Sec. III, we present the numerical results and related analysis. Finally, in Sec. IV we present our conclusions.

II. PHYSICAL MODEL AND THEORETICAL APPROACH

The SBEs, which govern the coupled dynamics of electrons, holes, and the optical polarization in the vicinity of the semiconductor band gap, provide a concrete foundation to analyze the optical properties of semiconductor structures. In the low-density limit, the SBE can be cast in real space as[45]

$$
i\hbar \frac{\partial \Psi(z,t)}{\partial t} = \left[E_g - \hbar^2 \frac{\partial^2}{\partial z^2} + ezF(t) - i\hbar\Gamma \right] \Psi(z,t) \\
- V_{\text{Coul}}(z)\Psi(z,t) + \hbar\Omega(t)\delta(z),
$$
(1)

where Ψ is the induced polarization between the lowest valance and conduction subbands, $\hbar$ is the Planck constant, z is the relative distance between the electron and the hole, $V_{\text{Coul}}(z)$ is the effective Coulomb potential which is calculated by averaging the three-dimensional Coulomb interactions through the wave functions of electrons and holes over the radial two-dimensional section and the specific form of $V_{\text{Coul}}(z)$ is given below, $\Omega(t)=dE(t)/\hbar$ is the time-dependent

Rabi frequency with d the interband dipole moment and $E(t)$ the envelope of the weak probe optical pulse, and Γ is the phenomenological dephasing rate due to various dephasing scattering in the quantum wire. The external electric field may include static and ac components, i.e., $F=F_{\text{dc}}+F_{\text{ac}}\cos(2\pi\nu_{\text{THz}}t+\varphi)$, where $\nu_{\text{THz}}=\omega_{\text{THz}}/2\pi$ is the frequency of the terahertz electric field and φ is the phase of the terahertz ac field at the time when the optical pulse reaches its peak value. The Fourier transform of Eq. (1) is exactly equivalent to the SBE in the low-density limit in k space. We assume that the exciting optical pulse is resonant with the band gap and hence the detuning does not appear explicitly.

Here, we concentrate on a two-subband semiconductor model and assume the quantum wire is cylindrical in a geometric profile. We assume perfect confinement at the ends in the growth direction and at a lateral wall. The infinite potential at the lateral wall of the thin cylindrical nanowire implies the envelope of the lateral ground-state wave functions of the electrons and holes are the Bessel function of zero order $J_0(\rho_{e(h)})$, where ρ_e and ρ_h are the radial coordinates of the electron and hole, respectively. Only considering the fundamental electron and hole subbands, the quasi-one-dimensional Coulomb interaction $V_{\text{Coul}}(z)$ can be obtained from the average of the three-dimensional Coulomb interaction with the lateral ground state by[28,40,46]

$$
V_{\text{Coul}}(z) = \kappa \int_0^R \int_0^R \int_0^{2\pi} \int_0^{2\pi} \frac{\rho_e \rho_h J_0^2\left(\frac{\alpha_0 \rho_e}{R}\right) J_0^2\left(\frac{\alpha_0 \rho_h}{R}\right)}{\sqrt{z^2 + \rho_e^2 + \rho_h^2 - 2\rho_e\rho_h\cos(\theta_h - \theta_e)}} d\rho_e d\rho_h d\theta_e d\theta_h,
$$
(2)

where $\kappa = e^2/[4\pi^3\varepsilon R^4 J_1^4(\alpha_0)]$, ε is the dielectric constant, R is the radius of the quantum wire, θ_e and θ_h are the polar angle coordinates of the electron and hole, respectively, J_1 is the Bessel functions of order 1, and α_0 is the zero of the J_0. The relevant observable in a usual experiment is the absorption coefficient, which can be obtained from the real and imaginary parts of the complex dielectric function $\epsilon(\omega) = \epsilon'(\omega) + i\epsilon''(\omega)$ as

$$
\alpha(\omega) = \frac{\omega}{n(\omega)c}\epsilon'',
$$
(3)

where ω is angular frequency and $n = \sqrt{\frac{1}{2}\{\epsilon'(\omega) + \sqrt{[\epsilon'(\omega)]^2 + [\epsilon''(\omega)]^2}\}}$ is the index of refraction. On the other hand, the complex dielectric function $\epsilon(\omega)$ is related to the linear optical susceptibility $\chi(\omega)$ via $\epsilon(\omega)=1+4\pi\chi(\omega)$. The optical polarization is simply $P(t)=d\Psi(z=0,t)$. The linear optical susceptibility $\chi(\omega)$ is finally calculated by

$$
\chi(\omega) = \frac{P(\omega)}{\varepsilon_0 E(\omega)},
$$
(4)

where $P(\omega)$ and $E(\omega)$ are the Fourier transformation of $P(t)$ and $E(t)$, respectively. In our calculations, the optical field is assumed to be polarized along the axis of the quantum wire. And we assume the optical pulse has a Gaussian slowly varying envelope $E(t)=E_0\exp[-(t-t_0)^2/\sigma^2]$ with σ the pulse width and t_0 the time at which the optical pulse is maximum. Thus only pulsed excitation is considered in this paper. If continuous excitation is concerned, we can employ the multipulse technique used in Refs. 27 and 28.

III. NUMERICAL RESULTS AND DISCUSSIONS

The cylindrical quantum wire is 4200 nm in length corresponding to about $300a_0$ with a_0 the effective Bohr radius of the bulk excitons in GaAs, and the radius of the wire is 4.2 nm. We employ material parameters typical of GaAs: $m_e=0.067m_0$ and $m_h=0.408m_0$ with m_0 the mass of a free electron, and $\varepsilon=12.9$ is the relative dielectric constant. The dephasing time is $\Gamma^{-1}=500$ fs unless otherwise stated. For the electric field of optical pulse, we choose a weak Gaussian pulse with the full width at half maximum 30 fs and t_0 510 fs. We use the center difference of the space with grid
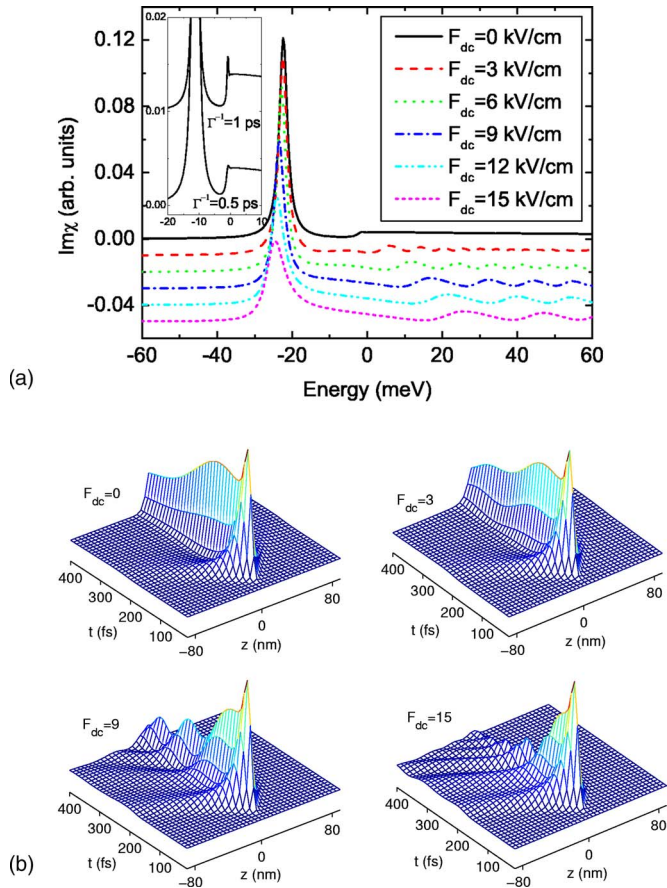
FIG. 1. (Color online) (a) Optical absorption spectra of the cylindrical quantum wire under different field strengths. The field strength F_{dc} varies from 0 to 15 kV/cm at the step of 3 kV/cm from top to bottom. The inset of (a) shows the 2s exciton peak for dephasing time Γ^{-1} 1 ps (top) and 0.5 ps (bottom), respectively. (b) The spatiotemporal evolution of the polarization wave packet under increasing electric fields. The four panels of (b) are spatiotemporal evolution of the polarization wave packet at different field strengths $F_{dc}=0$, 3, 9, and 15 kV/cm.

spacing 1 nm. And the SBE is integrated over 6 ps with a time step 0.1 fs. The total integration time is chosen in such a way that the initial polarization practically becomes zero at the end of integration. Usually $6-8/\Gamma$ is used as the upper limit. Thus 6 ps is used in the calculations in this paper. In addition, we have checked that the convergence of all results presented in this paper is ensured with respect to this discretization. However, when the statistic electric field is higher beyond 15 kV/cm, the discretization has to be improved further. This is because the field-induced ionization dominates the dephasing, thus a higher resolution of time and space is needed. The phase φ is chosen zero other than in the Fig. 3(b), where the phase dependence is investigated.

In Figs. 1(a) and 1(b), we show the optical absorption and the spatiotemporal evolution of the polarization wave packet in the cylindrical quantum wire under external dc electric fields, respectively. Figure 1(a) shows the optical absorption spectra at different electric field strength. The curves have been shifted vertically for clarity. In the absence of the electric field, the optical absorption spectrum is dominated by the

main exciton peak, and the absorption continuum is suppressed, thus the Sommerfield factor is less than unity. The 1s exciton binding energy is about 23.6 meV, which is about two times the exciton binding energy calculated for harmonic potential[42,43] and is in accord with the calculated result for a cylindrical quantum wire.[47] The Coulomb interaction between the electron and hole removes the singularity at the band gap associated with the one-dimensional joint density of states. The inset shows that the 2s exciton in the absence of external electric field is easily resolved, especially when the dephasing time is 1 ps. Note that the 2s exciton is very difficult to obtain by using the SBE approach in k space because of the numerical requirements for a long dephasing time. In the presence of an external electric field, the 1s exciton peak reduces in height, broadens in width, and its location shifts to lower energy, and the 2s exciton is completely ionized. The free carrier continuum portion of the spectra above the band-gap edge exhibits pronounced oscillations, which are the well known FK oscillations. The oscillation period is longer for a stronger electric field, while the oscillations decrease in amplitude for higher energies. Figure 1(b) shows the spatiotemporal evolution of the polarization wave packet under dc electric field with different field strengths: 0, 3, 9, and 15 kV/cm, respectively. The time ranges from 0 to 400 fs (corresponding to 51 fs advanced and 349 fs retarded to the center of the optical pulse). And the spatial range is −84 to 84 nm, which is approximately 100a_0. The spatiotemporal dynamics of the wave packet highlight the physics: shortly after the pulse arrives, there is a sharp peak near the center of the relative motion space due to the Coulombic interactions between electrons and holes. The wave packet spreads and quantum beating occurs between the continuum states and the excitonic states later on. The wave packet ultimately spreads out and dephases. In the absence of an external field ($F=0$ kV/cm), the polarization wave packet evolves symmetrically about the z direction, as expected. But, in the presence of an external field ($F\neq0$), the polarization wave packet is now strongly distorted and propagates along the negative z axis. The frequency of the quantum beating is higher for stronger fields, and the wave packets decay rapidly, which suggests the field-induced ionization of the exciton.

The optical absorption spectra of the cylindrical quantum wire and the spatiotemporal evolution of the polarization wave packet under external terahertz electric fields with different field strengths are shown in Figs. 2(a) and 2(b), respectively. Figure 2(a) shows the optical absorption spectra for different values of the field strength with frequency fixed at $\nu_{THz}=5$ terahertz, which is about resonant with the 1s exciton. The spectra are offset vertically for clarity. With the field strength increasing, the main exciton peak splits, and the two peaks are asymmetric both in height and width except for the field strength 9 kV/cm, where the two peaks are approximately symmetric. When field strength is lower than 9 kV/cm, the peak at the high-energy side is dominant over the one at the low-energy side. On the other hand, when field strength is higher than 9 kV/cm, the peak at the low-energy side is dominant over the one at the high-energy side, and the two peaks separate farther, and broaden, even becoming a band, and other peaks and oscillations emerge gradually.
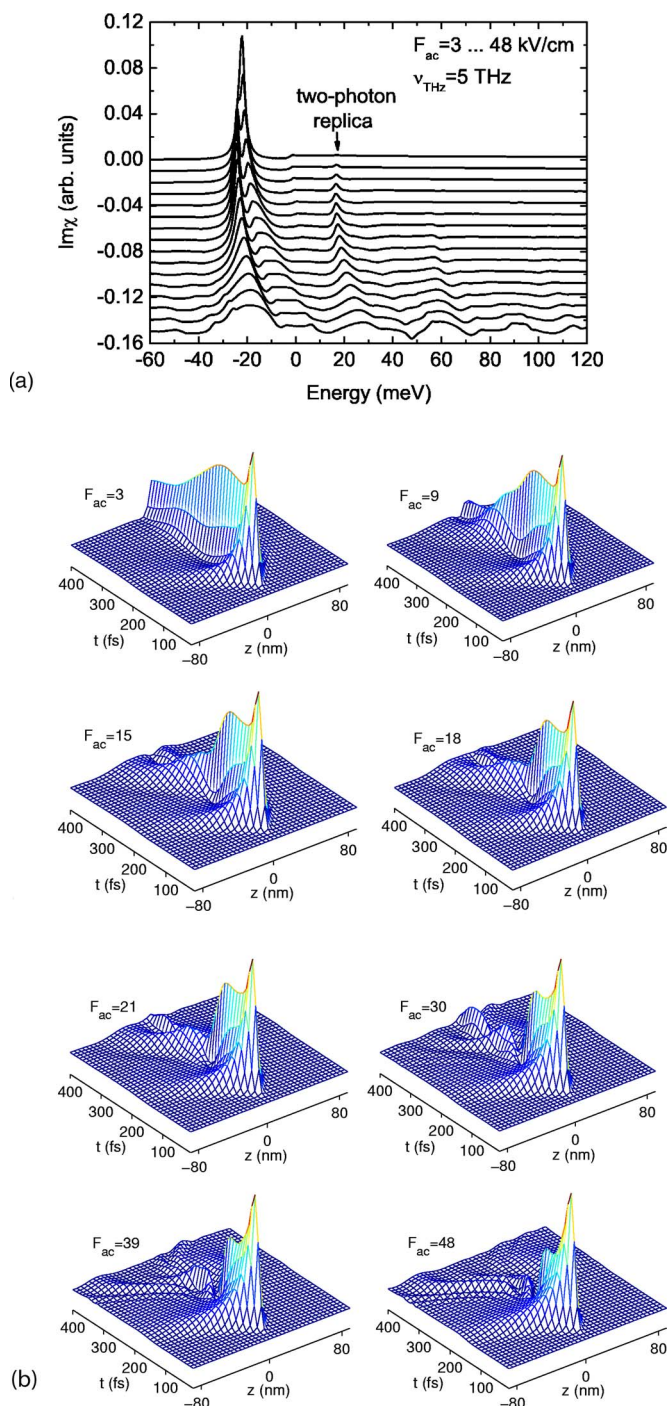
FIG. 2. (Color online) (a) Optical absorption spectra of the cylindrical quantum wire under terahertz electric fields. The field strength F_{ac} varies from 3 to 48 kV/cm at the step of 3 kV/cm from top to bottom with frequency ν_{THz} of the terahertz field fixed at 5 THz. (b) The spatiotemporal evolution of the polarization wave packet when increasing the field strength with frequency ν_{THz} =5 THz. The eight panels correspond to different field strengths F_{dc}=3, 9, 15, 18, 21, 30, 39, and 48 kV/cm, respectively.

This splitting resembles the Autler-Townes splitting for three level atoms,[48] whereas the third level coherently couples to one of the other two levels, resulting in a large dip in the absorption resonance. Here, the third level is played by the
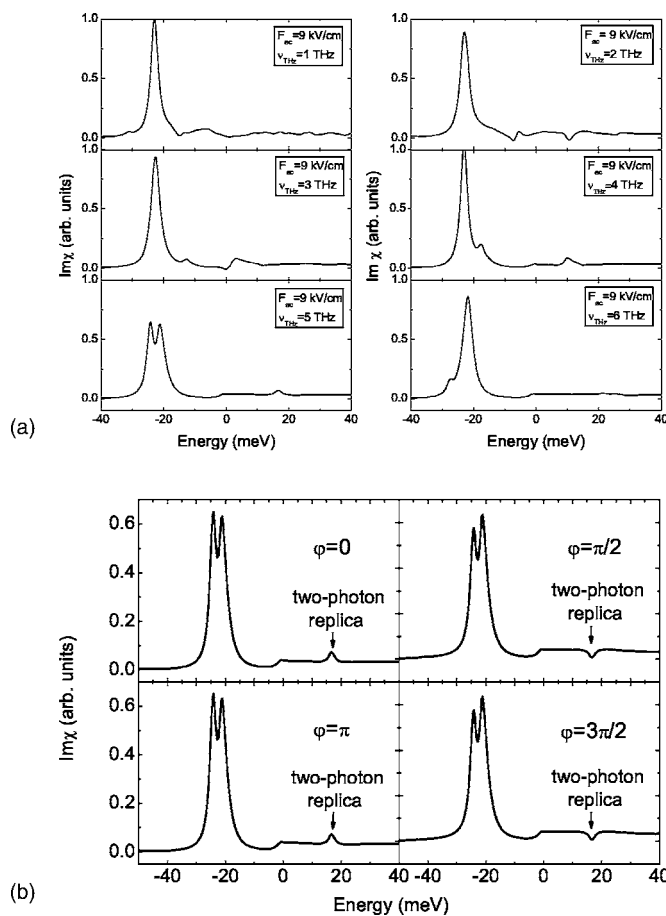

FIG. 3. (a) Optical absorption spectra of the cylindrical quantum wire under terahertz electric fields at different frequency ν_{THz}=1, 2, 3, 4, 5, and 6 THz with field strength fixed at 9 kV/cm, respectively. (b) Dependence of the optical absorption spectra of the cylindrical quantum wire on the phase under terahertz electric fields F_{ac}=9 kV/cm and ν_{THz}=5 THz. The four panels of (b) correspond to φ=0, $\pi/2$, π, and $3\pi/2$, respectively, with φ the phase of the terahertz wave at the time corresponding to the peak of the optical pulse.

higher exciton states lying just below the band edge. Furthermore, the 2s resonance and the band-edge blueshifts due to the dynamical FK effect. There appear two-photon replicas in the continuum. With the terahertz field increasing, the two-photon replica redshifts initially and turns into a blueshift and broadens. This is because the ac-Stark effect and dynamical FK effect oppose each other. The former redshifts the resonance, while the dynamical FK effect seeks to blueshift it. Eventually, the dynamical FK effect will dominate, resulting in a net blueshift. In very high field, the continuum becomes oscillating, and some other peaks corresponding to multiphoton replicas occur. Figure 2(b) shows the spatiotemporal dynamics of the polarization wave packet for some different values of the terahertz field strength. The polarization wave packet is distorted by the field and spreads to two directions following the alternating changing of the field. And there is a sharp drop for high field strength, which indicates the ionization of the excitons immediately after they are generated.

We show the dependence of optical absorption spectra on the phase and frequency of the terahertz field in the cylindrical quantum wire in Fig. 3. Figure 3(a) shows the influence of the frequency of the terahertz field on the main exciton peak. Note that the location of the dip in the split main $1s$ peak is one terahertz photon energy below the band edge. Thus, this splitting is a single terahertz photon resonance-induced coherent phenomenon. The separation and relative intensity are dependent on the frequency of a terahertz field. Multiphoton replicas can also be identified. Figure 3(b) shows the dependence of the absorption spectra on the phase φ of the terahertz field at the time when the probe optical pulse reaches its peak value. The four panels show the optical absorption spectra at the frequency $\nu_{THz}=5$ THz and the field strength $F_{ac}=9$ kV/cm with different phases of $\varphi=0$, $\pi/2$, π, and $3\pi/2$, respectively. The peak emerging in the absorption continuum is the two-photon replica which is $2h\nu_{THz}$ above the $1s$ excitonic resonance. By changing this phase, the absorption can be enhanced or reduced at the location of the two-photon replica. As Fig. 3 shows, the two-photon replicas are evident and can be easily tuned by changing the frequency and the phase of the terahertz driving field. This suggests the potential application of quantum wires as optical switching or multiplexing devices by employing the static-field-induced FK oscillations or the terahertz-field-induced FK effect and multiphoton replicas.

IV. CONCLUSIONS

In conclusion, we have studied the FK effect and dynamical FK effect in a cylindrical semiconductor quantum wire by solving the SBE in the low-density limit in real space. The spatiotemporal dynamics of the polarization wave packet under different field strengths are also presented. By probing the electron-hole wave-packet motion, exciton ionization effects have been highlighted. In the presence of a dc electric field, the $1s$ exciton peak reduces in height and broadens in width and the $2s$ exciton is completely ionized. For the reasonable dc electric field strengths, substantial oscillations appear above the band gap. In the presence of a terahertz field, the main $1s$ exciton peak is splitting and the relative height of the two peaks depends on the field strength. With increasing field strength, the dip redshift and the splitting peaks reduce and broaden and rich structures appear. Multiphoton replicas show up, and the two-photon replica depends evidently on the phase of the terahertz field.

ACKNOWLEDGMENTS

[1] S. Schmitt-Rink, D. S. Chemla, and D. A. B. Miller, Adv. Phys. **38**, 89 (1989).

[2] D. A. B. Miller, D. S. Chemla, T. C. Damen, A. C. Gossard, W. Wiegmann, T. H. Wood, and C. A. Burrus, Phys. Rev. Lett. **53**, 2173 (1984); Phys. Rev. B **32**, 1043 (1985).

[3] R. J. Elliott and R. Loudon, J. Phys. Chem. Solids **8**, 382 (1959); **15**, 196 (1969).

[4] T. Ogawa and T. Takagahara, Phys. Rev. B **44**, 8138 (1991); **43**, 14325 (1991).

[5] F. Rossi and E. Molinari, Phys. Rev. B **53**, 16462 (1996).

[6] F. Rossi, G. Goldoni, and E. Molinari, Phys. Rev. Lett. **78**, 3527 (1997).

[7] G. Ortner, I. Yugova, G. B. HogervonHogersthal, A. Larionov, H. Kurtze, D. R. Yakovlev, M. Bayer, S. Fafard, Z. Wasilewski, P. Hawrylak, Y. B. Lyanda-Geller, T. L. Reinecke, A. Babinski, M. Potemski, V. B. Timofeev, and A. Forchel, Phys. Rev. B **71**, 125335 (2005).

[8] C. Santori, M. Pelton, G. Solomon, Y. Dale, and Y. Yamamoto, Phys. Rev. Lett. **86**, 1502 (2001).

[9] C. Santori, G. S. Solomon, M. Pelton, and Y. Yamamoto, Phys. Rev. B **65**, 073310 (2002).

[10] S. V. Goupalov, R. A. Suris, P. Lavallard, and D. S. Citrin, IEEE J. Sel. Top. Quantum Electron. **8**, 1009 (2002).

[11] M. M. Dignam and J. E. Sipe, Phys. Rev. B **43**, 4097 (1991).

[12] D. M. Whittaker, Europhys. Lett. **31**, 55 (1955).

[13] C. P. Holfeld, F. Löser, M. Sudzius, K. Leo, D. M. Whittaker, and K. Köhler, Phys. Rev. Lett. **81**, 874 (1998).

[14] A. B. Hummel, T. Bauer, H. G. Roskos, S. Glutsch, and K. Köhler, Phys. Rev. B **67**, 045319 (2003).

[15] T. Y. Zhang, W. Zhao, and J. C. Cao, Phys. Rev. B **72**, 165310 (2005).

[16] S. Glutsch, *Excitons in Low-dimensional Semiconductors* (Springer, Berlin, 2004).

[17] W. Franz. Z. Naturforsch. A **13**, 484 (1958).

[18] L. V. Keldysh, Sov. Phys. JETP **34**, 788 (1958).

[19] A. P. Jauho and K. Johnsen, Phys. Rev. Lett. **76**, 4576 (1996).

[20] K. B. Nordstrom, K. Johnsen, S. J. Allen, A.-P. Jauho, B. Birnir, J. Kono, T. Noda, H. Akiyama, and H. Sakaki, Phys. Rev. Lett. **81**, 457 (1998).

[21] K. Johnsen and A.-P. Jauho, Phys. Rev. Lett. **83**, 1207 (1999).

[22] K. Johnsen, Phys. Rev. B **62**, 10978 (2000).

[23] A. V. Maslov and D. S. Citrin, Phys. Rev. B **62**, 16686 (2000).

[24] A. V. Maslov and D. S. Citrin, Phys. Rev. B **64**, 155309 (2001).

[25] C. J. Dent, B. N. Murdin, and I. Galbraith, Phys. Rev. B **67**, 165312 (2003).

[26] X. W. Mi, J. C. Cao, and C. Zhang, J. Appl. Phys. **95**, 1191 (2004).

[27] T. Y. Zhang and J. C. Cao, J. Phys.: Condens. Matter **16**, 9093 (2004).

[28] T. Y. Zhang, W. Zhao, J. C. Cao, and G. Qasim, J. Appl. Phys. **98**, 094311 (2005).

[29] T. Y. Zhang and J. C. Cao, J. Appl. Phys. **97**, 024307 (2005).

[30] D. S. Citrin, Phys. Rev. Lett. **82**, 3172 (1999); Appl. Phys. Lett. **76**, 3176 (2000); D. S. Citrin and S. Hughes, *ibid.* **78**, 1805 (2001).

[31] R. Rinaldi, R. Cingolani, M. Lepore, M. Ferrara, I. M. Catalano, F. Rossi, L. Rota, E. Molinari, P. Lugli, U. Marti, D. Martin, F. Morier-Gemoud, P. Ruterana, and F. K. Reinhart, Phys. Rev.

Lett. **73**, 2899 (1994).

[32] K. H. Wang, M. Bayer, A. Forchel, P. Ils, S. Benner, H. Haug, P. Pagnod-Rossiaux, and L. Goldstein, Phys. Rev. B **53**, R10505 (1996).

[33] W. R. Tribe, M. J. Steer, A. N. Forshaw, K. L. Schumacher, D. J. Mowbray, D. M. Whittaker, M. S. Skolnick, J. S. Roberts, and G. Hill, Appl. Phys. Lett. **73**, 3420 (1998).

[34] C. Constantin, E. Martinet, A. Rudra, and E. Kapon, Phys. Rev. B **59**, R7809 (1999).

[35] H. Akiyama, L. N. Pfeiffer, M. Yoshita, A. Pinczuk, P. B. Littlewood, K. W. West, M. J. Matthews, and J. Wynn, Phys. Rev. B **67**, 041302(R) (2003).

[36] S. Das Sarma and E. H. Hwang, Phys. Rev. B **54**, 1936 (1996).

[37] F. Tassone and C. Piermarocchi, Phys. Rev. Lett. **82**, 843 (1999).

[38] O. Mauritz, G. Goldoni, F. Rossi, and E. Molinari, Phys. Rev. Lett. **82**, 847 (1999).

[39] D. B. Tran Thoai and H. Thien Cao, Solid State Commun. **111**, 67 (1999).

[40] S. Das Sarma and D. W. Wang, Phys. Rev. Lett. **84**, 2010 (2000).

[41] T. G. Pedersen and T. B. Lynge, Phys. Rev. B **65**, 085201 (2002).

[42] S. Hughes and D. S. Citrin, Phys. Rev. Lett. **84**, 4228 (2000).

[43] S. Hughes, Phys. Rev. B **63**, 153308 (2001).

[44] S. Glutsch, D. S. Chemla, and F. Bechstedt, Phys. Rev. B **54**, 11592 (1996).

[45] H. Haug and S. W. Koch, *Quantum Theory of the Optical and Electronic Properties of Semiconductors*, 4th ed (World Scientific, Singapore, 2004).

[46] J. R. Madureira, P. A. Schulz, and M. Z. Maialle, Phys. Rev. B **70**, 033309 (2004).

[47] H. Ham and H. N. Spector, Phys. Rev. B **62**, 13599 (2000).

[48] S. H. Autler and C. H. Townes, Phys. Rev. **100**, 703 (1955).